THE JOURNAL OF PHYSICAL CHEMISTRY B

Article

pubs.acs.org/JPCB

Probing the Effect of miRNA on siRNA–PEI Polyplexes

Deniz Meneksedag-Erol,[†,§] Tian Tang,*[,†,‡] and Hasan Uludağ*[,†,§,⊥]

[†]Department of Biomedical Engineering, Faculties of Medicine & Dentistry and Engineering, University of Alberta, Alberta, Canada

[‡]Department of Mechanical Engineering, Faculty of Engineering, University of Alberta, Alberta, Canada

[§]Department of Chemical & Materials Engineering, Faculty of Engineering, University of Alberta, Alberta, Canada

[⊥]Faculty of Pharmacy and Pharmaceutical Sciences, University of Alberta, Alberta, Canada

Supporting Information

ABSTRACT: Delivery of small interfering RNA (siRNA) for silencing of aberrantly expressed genes is a promising therapy for the treatment of various genetic disorders. Polymeric carriers have been used in the design of efficient delivery systems to generate nanoscale siRNA polyplexes. Despite the great amount of research pursued on siRNA therapeutics, the underlying mechanisms of polyplex dissociation in cytosol are still unclear. The fate of siRNA polyplexes during intracellular stages of delivery and how the endogenous molecules may affect the integrity of polyplexes remains to be explored. In this study, we have focused on miRNA-21 as a representative anionic endogenous molecule and performed gel electrophoresis mobility shift assays, particle size and zeta (ζ)-potential analyses, and a series of all-atom molecular dynamics simulations to elucidate the effect of miRNA on siRNA–PEI polyplexes. We report a slightly better binding to PEI by miRNA than that of siRNA, and speculated that miRNA may disrupt the integrity of preformed siRNA–PEI polyplexes. In contrast to our initial speculation, however, introduction of miRNA to a preformed siRNA–PEI polyplex revealed formation of a miRNA layer surrounding the polyplex through interactions with PEI. The resulting structure is a ternary siRNA–PEI–miRNA complex, where the experimentally determined ζ-potential was found to decrease as a function of miRNA added.

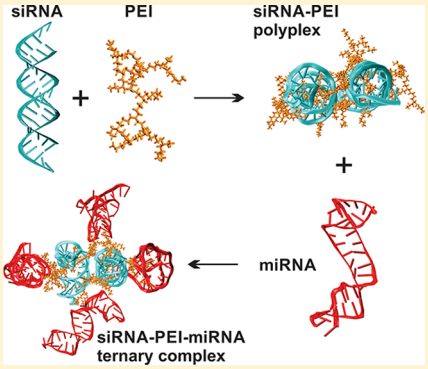

1. INTRODUCTION

Altering gene expression with the delivery of nucleic acids has been of great interest to researchers since the discovery of RNA interference (RNAi).[1] Post transcriptional gene silencing with the delivery of short interfering RNAs (siRNAs) has proven to be a promising approach in the treatment of cancer and various genetic disorders.[2] Challenges encountered in the use of siRNAs have led to a search for efficient delivery systems, and have driven the design of nonviral carrier vectors which assemble siRNAs into nanoscale complexes.[3] Among others, polymeric carriers have proven to be effective due to their capability to be engineered and functionalized at will. Polyethylenimine (PEI) is one of the most promising polycationic carriers bearing certain superior properties such as high buffering capacity (important for endosomal escape) and cellular uptake.[4] In an efficient delivery process, siRNAs get encapsulated by the carrier vectors to form polyplexes, which are then uptaken via endocytosis, followed by escape into cytosol and release of siRNAs from their carriers.[5] The guide strand in the siRNA can be recognized by Argonautes to form the core of the RNA-induced silencing complex (RISC)[6] only if siRNAs are released from their carriers. Although a large number of systematic studies have been conducted on the intracellular stages of the delivery process (see computational[7−10] and experimental[11,12] studies as examples), mechanistic details underlying the dissociation of polyplexes are yet to be explored.

One mechanism proposed for polyplex dissociation is based on the proton sponge effect[13] for carriers that possess a high H^+-buffering capacity like PEI. This mechanism suggests that PEI is able to resist pH changes within the endocytic vesicles due to having protonable amines.[4] During osmotic swelling and rupture of the vesicles containing PEI polyplexes, polyplex integrity might be affected and they may become prone to dissociation. However, controversial reports exist in the literature on the validity of this mechanism.[14,15] Irrespective of the proton sponge effect, the dynamic environment along the delivery pathway is likely to affect the integrity of polyplexes. Over the years, heparan-sulfate glycosaminoglycans (HSGAGs) have been used to test the stability of nucleic acid complexes *in vitro*. HSGAGs are complex polysaccharides located either on the cell membrane or in the extracellular matrix of eukaryotic cells. They are known for their role in cell signaling, tumor angiogenesis, and metastasis in a variety of cancer types by modulating cell–cell interactions.[16] Heparin, a highly sulfated member of the HSGAG family, has been widely adopted for testing the stability of polyplexes, and reported as an effective

Received: January 15, 2015
Revised: April 2, 2015
Published: April 6, 2015

DOI: 10.1021/acs.jpcb.5b00415
J. Phys. Chem. B 2015, 119, 5475−5486

binding agent to cationic carriers,[17−20] which competes with siRNA binding and can induce dissociation of polyplexes.

Bearing in mind that an efficient transfection requires polyplex dissociation upon endosomal escape, what triggers the release of siRNA from the carriers and the role of intracellular molecules on the integrity of polyplexes need to be understood. Since the electrostatic attraction between siRNAs and cationic carriers is the main driving force in the formation of polyplexes,[21] anionic intracellular molecules could be potent to destabilize the polyplexes. The microRNAs (miRNAs) are relatively short (∼22 nucleotides per strand) noncoding RNAs that are highly anionic. They are involved in many cellular processes, such as differentiation, apoptosis, and proliferation, and recently employed in transcriptional and post-transcriptional silencing of target genes.[22,23] miRNA-21 (miR-21) is one of the first identified mammalian miRNAs,[24] known to be aberrantly expressed in several types of cancers, e.g., breast, colon, lung, pancreas, prostate, and stomach, and its up-regulation is associated with carcinogenesis and tumor survival.[25] Considering its overexpression in cancers and anionic nature, miR-21 may have the capability of causing dissociation of delivered siRNA polyplexes.

In this work, we explore the effect of endogenous anionic molecules on the integrity of siRNA−PEI polyplexes using miR-21 as a representative molecule. Gel electrophoresis mobility shift assays (EMSA), particle size and zeta (ζ)-potential analyses, and a series of all-atom molecular dynamics (MD) simulations were performed in order to elucidate the role of miR-21 on polyplex dissociation. Our study aims to shed light on the fate of siRNA polyplexes in cytosol by simulating a more cell-like environment with the introduction of intracellular molecules and testing their effects with an experimental approach.

2. MATERIALS AND METHODS

2.1. Experimental. Two kDa PEI and heparin sodium from porcine intestinal mucosa (molecular weight of 17−19 kDa) were purchased from Sigma-Aldrich (St. Louis, MO). The polymer was dried by freeze-drying and reconstituted in distilled/deionized water at desired concentrations. Unlabeled and 5′-carboxyfluorescein (FAM)-labeled negative control siRNAs were purchased from Ambion (Austin, TX). The siRNA has the following sequence: sense strand, 5′-CAGAA-AGCUUAGUACCAAATT-3′; antisense strand, 5′-UUUGG-UACUAAGCUUUCUGTC-3′ (Figure 1a), with the ability of P-glycoprotein silencing.[26] MiRNA was purchased from Integrated DNA Technologies (IDT) (Coralville, IA). The sequence of miRNA is given in Figure 1b, except the synthesized miRNA comprises A−U Watson−Crick base pairs instead of G−U Wobble base pairs. SYBR Green II RNA gel stain (10 000× concentrate in DMSO) was purchased from Cambrex Bio Science (Rockland, ME).

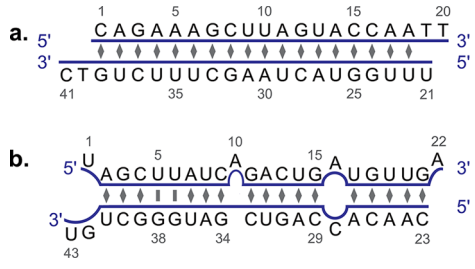

Figure 1. Schematic structures of (a) siRNA and (b) miRNA, simulated in this study. Watson−Crick base pairs are shown with diamonds, while Wobble base pairs are shown with rectangles.

PEI binding to siRNA and miRNA was investigated with EMSA and SYBR Green II dye exclusion assays. Polyplexes were prepared with 1 μg of control (scrambled) siRNA (in ddH_2O) or 1.5 μg of miRNA (in ddH_2O) incubated with various concentrations of 2 kDa PEI in 25 μL of 150 mM KCl for 30 min. For EMSA, samples were run on a 2% agarose gel containing 1 μg/mL ethidium bromide (100 V, 1 h) in duplicates. The gels were visualized under UV. The percentage of binding was calculated on the basis of the intensity of free siRNA or miRNA bands. For SYBR Green II dye exclusion assays, polyplexes were prepared as described above. A 100 μL portion of SYBR Green II solution (1:10 000 dilution in 150 mM KCl) was added to the polyplexes. The fluorescence of the samples was measured using a Fluoroskan Ascent Microplate Fluorometer (λ_{ex}, 485 nm; λ_{em}, 527 nm). The percentage of binding was calculated on the basis of the fluorescence intensity relative to the siRNA or miRNA alone samples. Assays were run in triplicates, and the binding curves were generated by plotting the percentage of bound RNA versus PEI:RNA weight ratio.

The EMSA was also performed for the assessment of miRNA's effect on the integrity of siRNA−PEI polyplexes. Polyplexes were prepared with 0.3 μg of FAM−siRNA (in ddH_2O) and incubated with 2 kDa of PEI at PEI:siRNA weight ratio = 1 for 30 min. Various concentrations of miRNA were added onto the polyplexes, and the mixtures were further incubated for 1 h. Samples were run on a 2% agarose gel (100 V, 1 h) in duplicates. As a control, heparin was added to the polyplexes in the same way and run on the gel. The gels were visualized with a Fluoro Image Analyzer using a FAM filter. The percentage of dissociation was calculated from the fluorescence intensity of the dissociated bands to that of the free FAM−siRNA bands. Curves were generated by plotting the percentage of unbound FAM−siRNA versus the heparin/miRNA to FAM−siRNA mole ratio.

For the determination of particle size, two different PEI:RNA weight ratios were used for the polyplex formation: PEI:RNA = 0.3, corresponding to the weight ratio used in binding simulations, and PEI:RNA = 1, corresponding to the highest ratio used in binding experiments as well as in the experiments carried out for investigation of miRNA's effect on polyplexes. Polyplexes were either prepared in ddH_2O or in salt (150 mM KCl) with a final volume of 50 μL, by incubating 2 μg of control (scrambled) siRNA (in ddH_2O) or 3 μg of miRNA (in ddH_2O) with different concentrations of 2 kDa PEI for 30 min. To determine the effect of miRNA on the size of siRNA−PEI polyplexes, polyplexes were prepared with 2 μg of control (scrambled) siRNA as described above. Various concentrations of miRNA were added to the polyplexes, and the mixtures were further incubated for 1 h. For the determination of ζ-potential, samples were prepared in the same way as described above but only in ddH_2O. All the size and ζ-potential measurements were carried out in triplicates using a Zetasizer (Nano ZS; Malvern Instruments, U.K.).

2.2. Computational. The simulated siRNA is identical to what was used in experiments, shown in Figure 1a. It carries a total charge of −40 on its backbone phosphate groups in the fully deprotonated state. The simulated carrier is native branched PEI (Figure 2), which is composed of 43 amine groups, and has a molecular weight of 1874 Da. It possesses 20

DOI: 10.1021/acs.jpcb.5b00415
J. Phys. Chem. B 2015, 119, 5475−5486

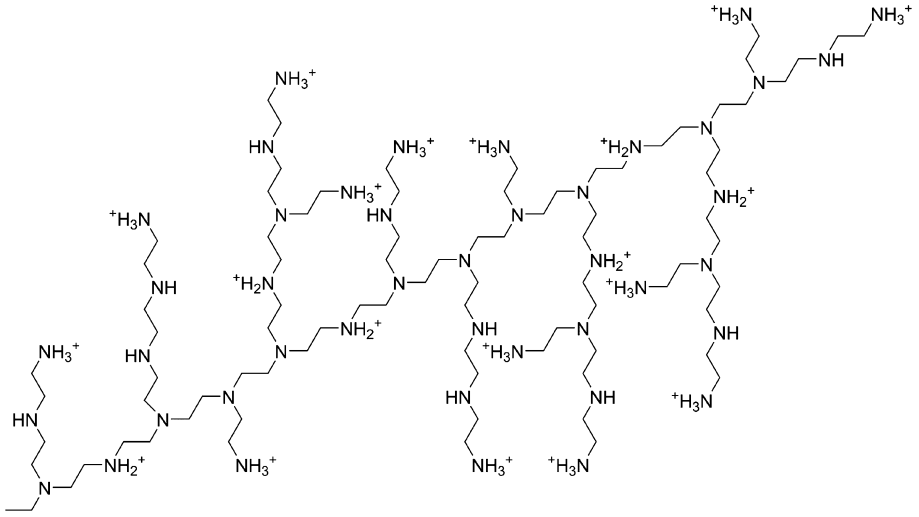

Figure 2. Molecular structure and protonation sites of the simulated PEI.

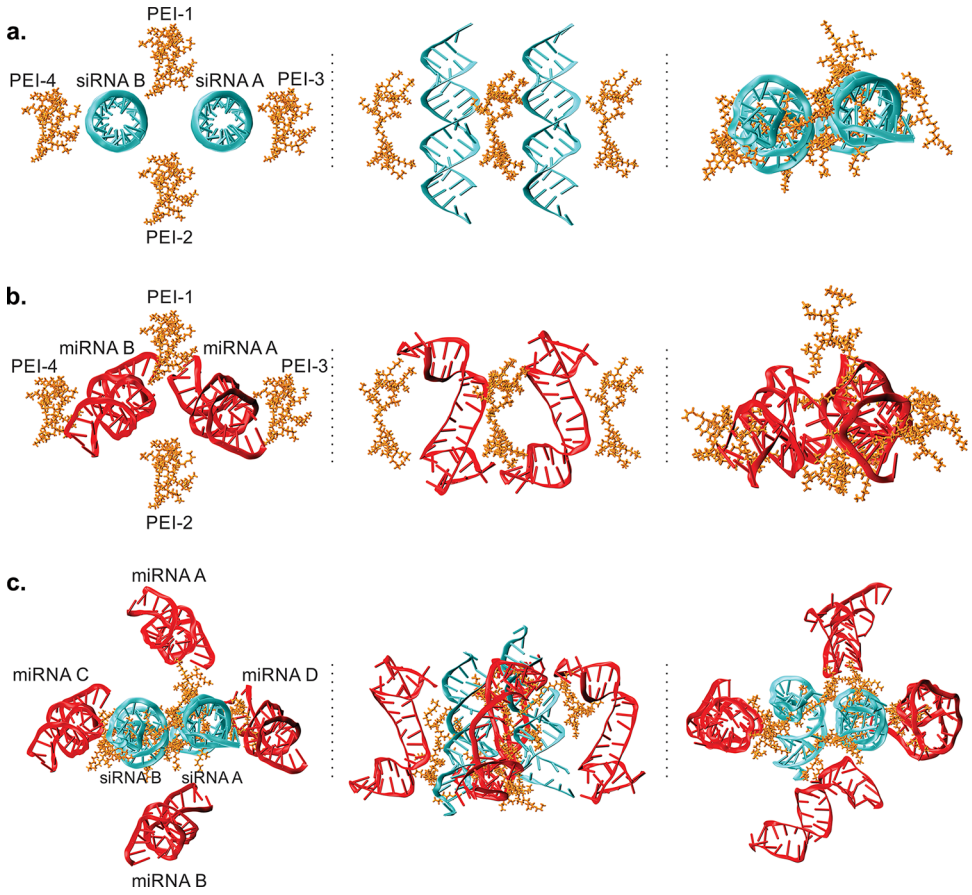

Figure 3. Initial (left panel, top view; middle panel, side view) and final (right panel, top view) configurations of the simulated systems: (a) 2s-4P, (b) 2m-4P, (c) 2s-4P-4m. siRNAs are given in cyan, while miRNAs and PEIs are represented in red and orange, respectively. Water and ions are removed for clarity.

protonated amine groups, corresponding to a protonation ratio of 47%, found experimentally at pH 6.[27] The simulated miRNA is mature miR-21,[24] which has the following sequence: sense strand, 5′-UAGCUUAUCAGACUGAUGUUGA-3′; antisense strand, 5′-CAACACCAGUCGAUGGGCUGU-3′. It bears two G−U Wobble base pairs, one bulge located at A10, and one mismatch located at A16 (Figure 1b). The total charge of the miR-21 is −41 in the fully deprotonated state. For the discussion purposes herein, miR-21 will be referred to simply as miRNA.

The initial structures (PDBs) of individual siRNA and PEI molecules were adopted from a previous study[28] published by our group. The topology for PEI molecules was developed and validated in a prior work[29] based on the CHARMM general force field,[30] while the CHARMM 27[31−34] force field was used for all other molecules. Pre-equilibration of PEI was carried out

DOI: 10.1021/acs.jpcb.5b00415
J. Phys. Chem. B 2015, 119, 5475−5486

Table 1. Information on the Three Simulated Systems in This Study

name	molecules simulated	number of atoms	size of simulation box (Å^3)	number of K^+/Cl^-	simulation time restrained + free (ns)
2s-4P	2 siRNA, 4 PEI	123 034	128 × 98 × 103	112/112	10 + 50
2m-4P	2 miRNA, 4 PEI	106 427	128 × 98 × 90	98/96	10 + 50
2s-4P-4m	2 siRNA, 4 PEI, 4 miRNA	220 971	147 × 147 × 108	363/199	10 + 100

earlier[28] in NAMD[35] for 50 ns, upon solvation with TIP3P water[36] and neutralization with the proper amount of Cl^- ions. siRNA was built with the AMBER NAB tool,[37] and used without any pre-equilibration due to its stability in aqueous environments.[28] The initial structure of miRNA was built with the make-na server (http://structure.usc.edu/make-na/) and pre-equilibrated for 60 ns in NAMD upon solvation with TIP3P water and neutralization with the proper amount of K^+ ions (see section S1 in the Supporting Information for details).

Two sets of simulations were performed to investigate (i) the binding of PEI to siRNA and miRNA and (ii) the effect of miRNA on the integrity of preformed siRNA−PEI polyplexes. For (i) binding studies, two simulations were performed with systems containing either two siRNAs (labeled as siRNAs A and B, see Figure 3a, left panel) or two miRNAs (labeled as miRNA A and B, see Figure 3b, left panel) and four PEI molecules (labeled as PEI 1, 2, 3, and 4; see Figure 3a and b, left panel). These two systems will be referred to as 2s-4P and 2m-4P, respectively. Each system was solvated in a cubic box with TIP3P water, and K^+ and Cl^- ions were added to obtain physiological salt conditions of 150 mM. Simulation was performed for 50 ns for each system. For the investigation of (ii) miRNA's effect on the siRNA−PEI polyplex, four miRNA molecules (labeled as miRNA A, B, C, and D; see Figure 3c, left panel) were introduced to the final configuration of the 2s-4P system at the end of the 50 ns dynamics; the system will be referred to as 2s-4P-4m. The same solvation procedure and salt concentration were adopted, and the simulation was performed for 100 ns. Table 1 lists the details of the three simulated systems. Initial configurations of the simulated systems are depicted in Figure 3 (left and middle panels). Different initial configurations were tested and shown not to affect the overall results (see section S2 in the Supporting Information for details).

All simulations were performed with NAMD[35] with a time step of 2 fs, periodic boundary conditions (PBC), and electrostatics with particle mesh Ewald (PME)[38] where grid sizes were defined manually on the basis of cell basis vectors (for systems 2s-4P, 2m-4P, and 2s-4P-4m, respectively, the grid sizes are PMEGridSizeX = 144, 144, 160; PMEGridSizeY = 100, 100, 160; and PMEGridSizeZ = 108, 96, 112). The cutoff for van der Waals and pairwise electrostatic interactions was set to 12 Å, and the SHAKE algorithm[39] was used to constrain bonds involving hydrogen atoms. Each system was first minimized for 5000 steps and then heated from 0 to 300 K with a harmonic restraint (10 kcal/mol·Å^2) on non-hydrogen atoms of the solute for 20 ps. After minimization and heating, the restraint was kept for 10 ns, and then removed for NPT simulations. Temperature and pressure control was carried out with a Langevin dynamics thermostat and a Nosé−Hoover Langevin barostat. The thermostat damping coefficient was set to 10 ps^{-1} for all non-hydrogen atoms. The barostat damping time scale was chosen to be 100 fs, and the oscillation period for the Langevin piston was set to 200 fs. The length of unrestrained NPT simulation for each system is given in Table 1. Trajectories were visualized and analyzed with VMD.[40]

3. RESULTS AND DISCUSSION

3.1. PEI Binding to siRNA and miRNA. PEI's binding ability to siRNA and miRNA was investigated with EMSA and SYBR Green II dye exclusion assays. Figure 4a shows the EMSA images of siRNA and miRNA binding to PEI (top panel), along with the percentage of bound RNA as a function of PEI:RNA weight ratio (bottom panel), quantified on the basis of the intensity of the siRNA/miRNA bands in the top

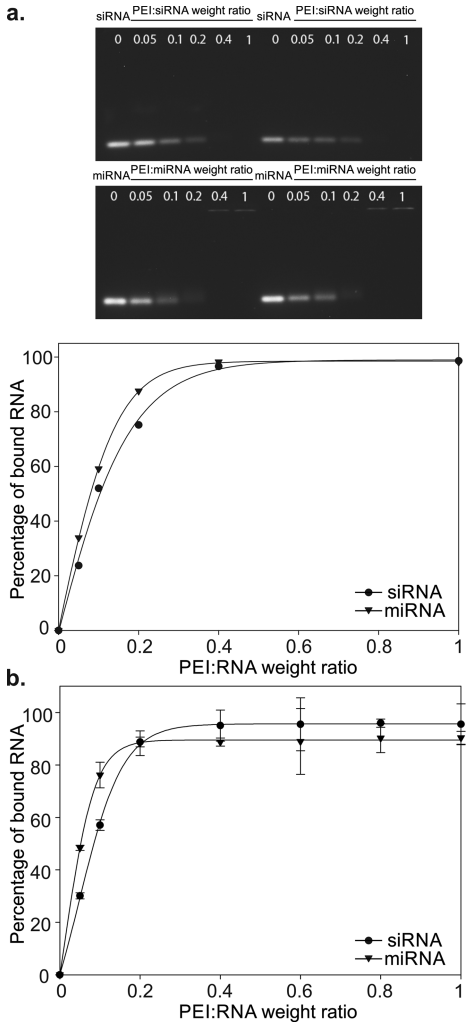

Figure 4. (a) Top panel: EMSA images of siRNA and miRNA binding to PEI. The first lane corresponds to the free siRNA or miRNA bands (PEI:RNA weight ratio = 0), while the PEI:RNA weight ratio was gradually increased in the following lanes. Data from the duplicate assays is given. Bottom panel: Percentage of siRNA or miRNA bound to PEI as a function of PEI:RNA weight ratio, quantified on the basis of the intensity of the free siRNA or miRNA bands. (b) Percentage of bound RNA as a function of the PEI:RNA weight ratio from SYBR Green II dye exclusion assays. For PEI:RNA weight ratios of 0, 0.05, 0.1, 0.2, 0.4, 0.6, 0.8, and 1, the corresponding N:P ratios are 0, 0.39, 0.79, 1.58, 3.16, 4.74, 6.32, and 7.90, respectively.

DOI: 10.1021/acs.jpcb.5b00415
J. Phys. Chem. B 2015, 119, 5475−5486

panel. As the PEI:RNA ratio increased, an increase in the bound siRNA and miRNA fraction was observed as expected, and 100% binding was achieved for both RNAs at approximately 1:1 weight ratio. At lower PEI:RNA weight ratios (<0.4), the percentage of bound miRNA was found to be higher than that of siRNA at a given weight ratio. These observations were further validated with SYBR Green II dye exclusion assays (Figure 4b), where the same binding trend was observed. Particularly, at PEI:RNA weight ratios of 0.05 and 0.1, respectively 48 and 76% of the miRNA are bound, while the corresponding data for siRNA are 30 and 57%. Both RNAs reach the same % binding (88%) at a PEI:RNA weight ratio of 0.2, and a plateau is observed beyond that point. The experimentally obtained plateau value is slightly higher for siRNA, but both plateau lines are within the standard deviations in this region.

From both EMSA and SYBR Green II dye exclusion assays, it is clear that miRNA shows slightly better binding to PEI at low PEI:RNA weight ratios. In order to investigate the atomistic details of PEI binding to siRNA and miRNA, MD simulations were carried out on siRNA and miRNA polyplexes. Simulation systems were designed at a PEI:RNA weight ratio of ∼0.3 in order to be consistent with the PEI:RNA weight ratio range tested in the experiments. The corresponding PEI:RNA charge ratio was 1. Parts a and b of Figure 3 (right panels) show the snapshots of the final configurations of the polyplexes formed by PEI binding to siRNAs and miRNAs, respectively. Visual examination of the snapshots revealed similar characteristics of polyplex formation. Specifically, in both cases, all PEIs were found to bind to and surround centrally sequestered siRNAs or miRNAs. To probe the compactness of the formed polyplexes, the radius of gyration (R_g) of the two siRNAs or miRNAs are plotted as a function of the simulation time (Figure 5a). A lower R_g value indicates a more compact RNA arrangement within the polyplex. Both R_g curves follow a decreasing trend within the first 20 ns of the simulations as a result of the polyplex formation, while, in the range 20−50 ns, they reach a plateau with some fluctuations. The average R_g values for the last 10 ns of the simulations are 23.08 ± 0.23 and 21.36 ± 0.20 Å for systems 2s-4P and 2m-4P, respectively, which indicates that system 2m-4P has a slightly more compact RNA arrangement compared to that of 2s-4P. Figure 5b shows the center of mass (COM) distances between the RNAs during the complexation. The COM distances start from 35.5 Å, which was the distance between the RNAs set in the initial configuration of 2s-4P and 2m-4P systems. Both curves follow a decreasing trend within the first ∼20 ns. Fluctuations appear between 20 and 45 ns, and both curves reach a plateau at ∼45 ns. The average COM distance values for the last 10 ns of the simulations are 26.96 ± 0.74 and 25.45 ± 0.45 Å for systems 2s-4P and 2m-4P, respectively. In agreement with the trend observed for R_g in Figure 5a, the COM distance of miRNAs in system 2m-4P is slightly lower than the COM distance of siRNAs in system 2s-4P, which confirms the formation of a slightly more compact RNA arrangement in the 2m-4P system. To investigate the potential reason behind this observation, root-mean-square deviations (RMSDs) of the non-hydrogen atoms of the individual RNAs with respect to their initial configurations are plotted as a function of the simulation time (Figure 5c). All four RMSD curves follow an increasing trend due to the motion of RNAs during polyplex formation within the first ∼20 ns. The average RMSD values of individual RNAs for the last 10 ns of the simulations are 4.21 ± 0.31 Å for siRNA A and 3.63 ± 0.58 Å for siRNA B in system 2s-4P and 6.73 ± 0.16 for miRNA A and 9.34 ± 0.31 Å for miRNA B in system 2m-4P, respectively.

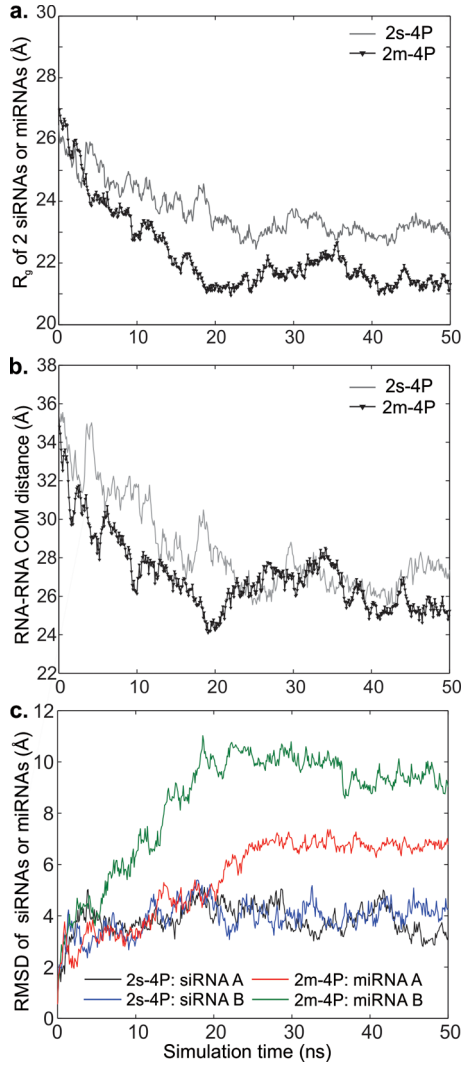

Figure 5. (a) R_g of two siRNAs and miRNAs; (b) RNA−RNA COM distance; (c) RMSD of the non-hydrogen atoms of individual siRNAs and miRNAs with respect to their initial configurations. Data are plotted as a function of simulation time. In parts a and b, each subfigure contains two curves, corresponding to 2s-4P and 2m-4P systems, respectively, and in part c, there are four curves corresponding to each RNA in 2s-4P and 2m-4P systems.

Larger deviation observed in the 2m-4P system indicates larger deformation and structural fluctuation of the miRNA. This observation could be attributed to bulge and mismatch regions in the miRNA, which lead to the loss of H-bonding network between base pairs (see section S1 in the Supporting Information for details). The larger deformation of miRNA accommodated PEI better, so that a more compact miRNA arrangement in the polyplex was obtained.

Previous MD simulations[41] indicated PEI's role in polynucleotide aggregation to be twofold: (i) formation of polyion bridges between different polynucleotide segments and (ii) screening of polynucleotide charges. PEI's role in aggregating siRNA and miRNA was investigated on the basis of these mechanisms. First, to explore polyion bridging, in Figure 6, we plot the number of PEI N atoms within 4 Å of any N/O atoms of siRNA or miRNA, as a function of simulation time. The 4 Å

DOI: 10.1021/acs.jpcb.5b00415
J. Phys. Chem. B 2015, 119, 5475−5486

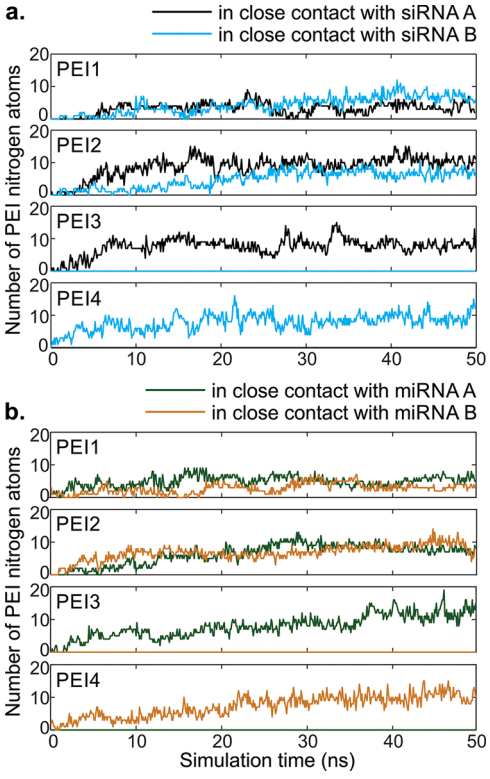

Figure 6. Number of nitrogen atoms for each PEI within 4 Å of any (a) siRNA and (b) miRNA N/O atoms as a function of simulation time. Four plots in each subfigure correspond to four PEIs, and two curves in each plot correspond to two siRNAs or miRNAs.

limit was chosen, as it is the distance for a direct H-bond to be formed between a PEI amine group and a RNA N/O atom.[28] Each subfigure consists of four plots that correspond to the four PEIs in the system (numbered in Figure 3a,b, left panel), and each plot contains two curves each representing one RNA (siRNA or miRNA) molecule (labeled in Figure 3a,b, left panel). In the initial configurations, PEI-1 and PEI-2 are located in the region between two RNA molecules, while PEI-3 and PEI-4 are, respectively, on the right- and left-hand sides of the RNAs. To quantify polyion bridging, a PEI N is said to be in close contact with a RNA if it is within 4 Å of an siRNA or miRNA N/O atom. A PEI is said to be bound to a RNA if it has at least one N atom in close contact with the RNA. A polyion bridge is said to be formed if one PEI is simultaneously bound to more than one RNA molecule. From Figure 6, it can be seen that, after 20 ns, the binding of PEIs to both RNAs shows a very similar pattern. Specifically, PEI-1 and PEI-2 are found to bridge the two RNA molecules, whereas PEI-3 and PEI-4 are only bound to one of the RNAs: PEI-3 to siRNA A or miRNA A and PEI-4 to siRNA B or miRNA B. Quantitatively, the numbers of PEI N's in close contact with a RNA are also comparable in the two cases. The observation on the interactions of PEI-3 and PEI-4 only with their nearest RNA is the consequence of initial placement of PEIs. No apparent difference was found between siRNA and miRNA polyplexes in PEI binding dynamics, indicating that polyion bridging is not affected by the type of the RNA, given similar size, charge density, and initial configuration of the RNAs.

In order to probe the electrostatic screening of RNA charges, cumulative distributions of PEI N^+, K^+, and Cl^- atoms as well as their total net charge are plotted as a function of the distance from any siRNA (Figure 7a) or miRNA (Figure 7b) C1′ atoms, averaged over the last 10 ns of the simulations. In each

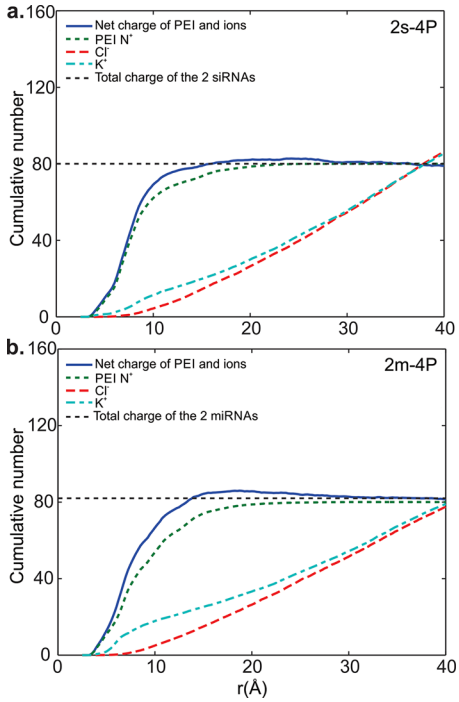

Figure 7. Cumulative numbers of PEI N^+, K^+, and Cl^- atoms and the total net charge of PEI and ions as a function of the distance from any (a) siRNA or (b) miRNA C1′ atoms, averaged over the last 10 ns of the simulations. Total charges of −80 of the two siRNAs (a) and −82 of the two miRNAs (b) are plotted by black dashed lines as reference.

subfigure, the black dashed line indicates the negative charge coming from the two siRNAs (80 in Figure 7a) or from the two miRNAs (82 in Figure 7b). The blue solid curve stands for the total net charge coming from all the charged entities in the system, except the RNAs, within the given range. Intersection of the black dashed line and the blue solid curve indicates the point of 100% neutralization of RNA charges. For system 2s-4P, 100% neutralization occurs at a distance of 15.99 Å (Figure 7a), while, for system 2m-4P, it occurs at a shorter distance of 13.88 Å (Figure 7b). RNAs are overneutralized if the total charge coming from PEI N^+ atoms and K^+ and Cl^- ions exceeds the total charge of RNAs, i.e., when the blue solid curve becomes above the black dashed line. It can be seen that for both systems overneutralization occurs, reaching a maximum at 24.25 Å for 2s-4P (Figure 7a) and at 18.75 Å for 2m-4P (Figure 7b) systems. Although the characteristics of neutralization are similar for the two systems, slight differences exist in the number of individual types of atoms. At short distances (<7 Å), the number of PEI N^+'s is higher in the 2m-4P system than in 2s-4P. In contrast, in the range of 7 Å < r < 14 Å, the number of PEI N^+'s becomes higher in 2s-4P than in 2m-4P, and at large distances (14−40 Å), they are similar to each other. The number of K^+ ions is higher in 2m-4P than in 2s-4P until 28 Å, while the trend changes to 2s-4P > 2m-4P in the range 28−40 Å. The number of Cl^- ions follows a similar trend in both systems up to 28 Å, while they become higher in 2s-4P than 2m-4P afterward. Irrespective of the differences in the number of individual types of atoms, the net charge of PEI and ions (blue solid curve) determines the point of 100% neutralization of RNA charges. Neutralization of miRNA charges at a shorter

DOI: 10.1021/acs.jpcb.5b00415
J. Phys. Chem. B 2015, 119, 5475−5486

distance shows slightly better screening capability of PEI and ions in the 2m-4P system in comparison to the 2s-4P system.

Computational observations on the slightly better binding of miRNA to PEI as compared to siRNA binding to PEI are in agreement with experiments. These results led us to ask the question, can miRNAs attract PEIs in a preformed siRNA−PEI polyplex and cause polyplex dissociation? This hypothesis was investigated via experiments and simulations below.

3.2. Effect of miRNA on siRNA−PEI Polyplex Integrity. In order to examine the effect of miRNA on the integrity of the siRNA−PEI polyplex experimentally, EMSA was performed with the addition of miRNA into preformed FAM−siRNA−PEI polyplexes. Heparin was used as a reference, due to its well-known capability of dissociating polyplexes. The concentration of miRNA or heparin added onto preformed polyplexes was gradually increased, and the intensity of the fluorescence signal was quantified to calculate the amount of unbound FAM−siRNA (Figure 8). At heparin:FAM−siRNA and miRNA:-FAM−siRNA mole ratios of 1.55 and 2.05, respectively, we have observed 56% of FAM−siRNA dissociated by heparin, while no FAM−siRNA release is apparent with miRNA. Further increase in the mole ratio (≥3) resulted in 98−100% of FAM−siRNA to be released by heparin; however, miRNA addition only resulted in 5% FAM−siRNA release, even at the highest ratio (=8.18). In addition, starting from a miRNA:-FAM−siRNA mole ratio of 4.2, some miRNAs were observed to float freely in solution (data not shown) instead of participating in binding to or dissociating the preformed FAM−siRNA polyplex.

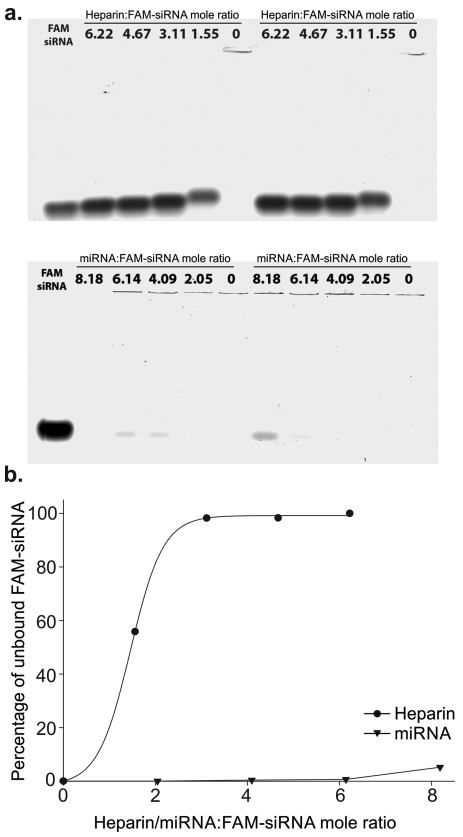

Figure 8. (a) EMSA images of FAM−siRNA release from FAM−siRNA−PEI polyplex by heparin (top panel) and miRNA (bottom panel). The heparin/miRNA:FAM−siRNA mole ratio is gradually increased from right to left, while the leftmost lane corresponds to FAM−siRNA only (no PEI, heparin, or miRNA). Data from the duplicate assays is given. (b) Analysis of the unbound FAM−siRNA (%) as a function of heparin/miRNA:FAM−siRNA mole ratio, quantified on the basis of the intensity of free FAM−siRNA bands provided in part a. The mole ratios were calculated by assuming molecular weights of 18 and 13.7 kDa for heparin and miRNA, respectively, and a molecular weight of 14 kDa for siRNA.

We further investigated the effect of miRNA addition on the size and ζ-potential of siRNA−PEI polyplexes. First, siRNA−PEI and miRNA−PEI polyplexes were prepared at two different PEI:RNA weight ratios, 0.3 and 1, corresponding to the ratio used in binding simulations and the maximum ratio used in experiments, respectively, and measurements were conducted in 150 mM KCl and ddH_2O. In 150 mM KCl, the particles were 350−500 nm for siRNA−PEI and 600−750 nm for miRNA−PEI systems (Figure 9a). Increasing PEI:RNA weight ratio resulted in no significant changes in size. As the environment changed from 150 mM KCl to ddH_2O, we observed a decrease in particle sizes, except for PEI:siRNA = 1 (Figure 9b). Electrostatic screening in the presence of ions might have resulted in larger particles. When miRNAs were gradually introduced into siRNA−PEI polyplexes, particles remained intact (Figure 9c). It has to be noted that size fluctuations were observed, particularly in the polyplexes prepared at PEI:siRNA weight ratio = 1. However, no significant change was detected in the hydrodynamic diameter of the polyplexes which would be indicative of polyplex dissociation. With the gradual addition of miRNA, the ζ-potential (Figure 9d) decreased for polyplexes prepared at both PEI:siRNA weight ratios, reaching the final charge of −27 and −29.6 for PEI:siRNA weight ratio = 0.3 and 1, respectively. These observations show that miRNAs do not trigger polyplex dissociation but rather possibly lead to the formation of an outer layer surrounding the siRNA−PEI polyplex.

In order to test our hypothesis on the formation of ternary siRNA−PEI−miRNA structures, a simulation was performed by introducing four miRNA molecules into the final configuration of the 2s-4P system, so as to surround the preformed siRNA−PEI polyplex symmetrically (Figure 3c, left and middle panels) and form the 2s-4P-4m system. The 2s-4P-4m system was simulated for 100 ns, and visual examination of the complex structure at the end (Figure 3c, right panel) revealed that, although contacts were formed between miRNAs and PEIs, the siRNA polyplex remained intact and no apparent loosening of the polyplex was visible.

To quantify the compactness of siRNA arrangement upon miRNA introduction, R_g of the two siRNAs in the 2s-4P-4m system is plotted as a function of the simulation time (Figure 10). At the beginning of the simulation (after the minimization and restrained dynamics), R_g is found to be 22.83 Å, which is almost the same as the final R_g of the 2s-4P system, 22.90 Å. Although fluctuations are apparent during the entire simulation, a plateau is reached in the last 20 ns. The average R_g for the last 20 ns is 22.21 ± 0.12 Å, which is very close to the initial value. Therefore, although our earlier simulations showed slightly better binding of miRNA to PEI, their addition into a preformed siRNA−PEI polyplex did not loosen the compact arrangement of the siRNAs.

On the other hand, Figure 3c (right panel) revealed the formation of contacts between miRNAs and PEIs, and attachment of miRNAs to the periphery of the polyplex. Dynamics of PEI binding to both RNAs was probed for system 2s-4P-4m (Figure 11), with the same procedure described in

DOI: 10.1021/acs.jpcb.5b00415
J. Phys. Chem. B 2015, 119, 5475−5486

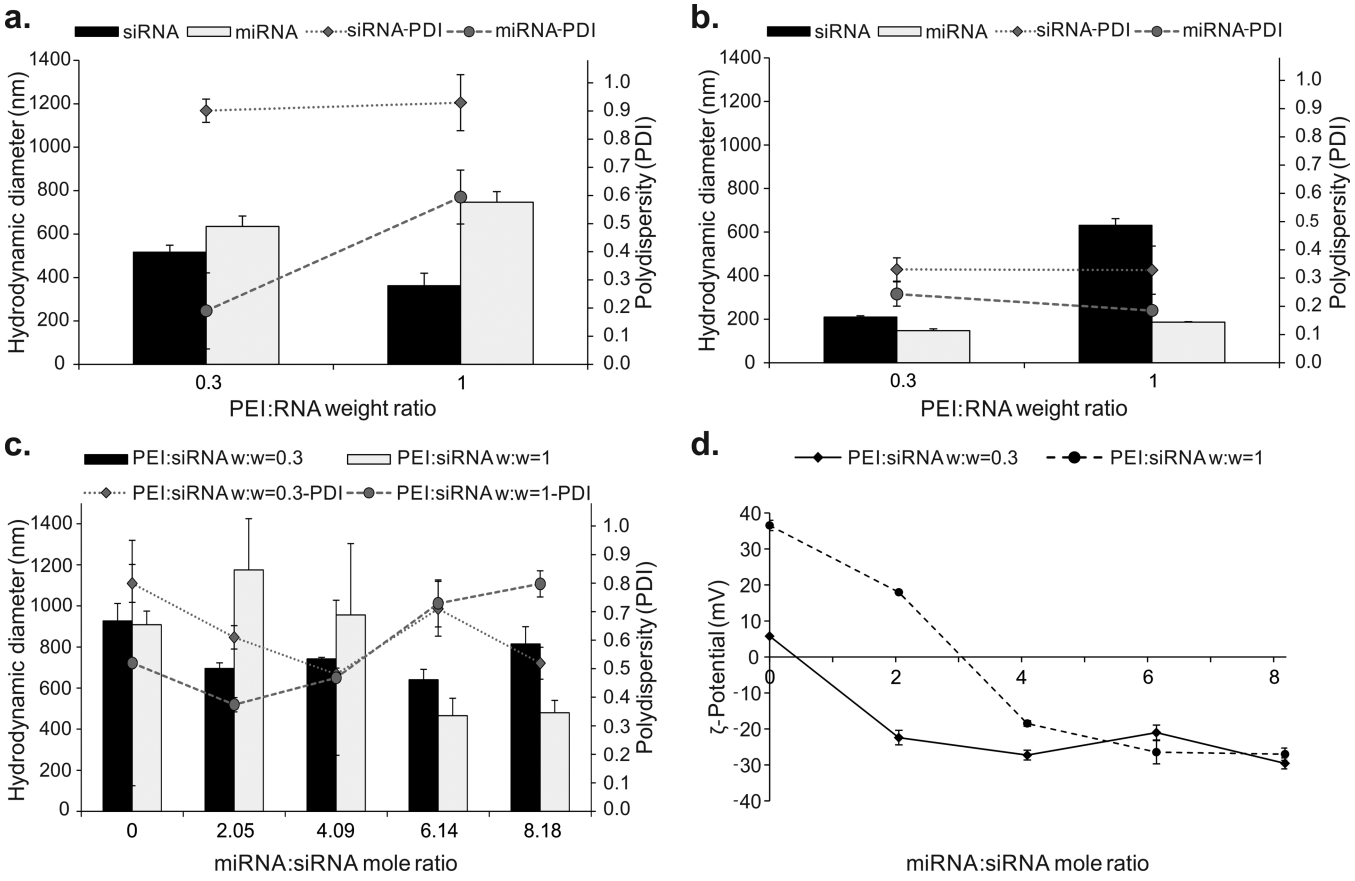

Figure 9. Hydrodynamic diameter of the polyplexes prepared at PEI:RNA weight ratios of 0.3 and 1, as measured in (a) 150 mM KCl and (b) ddH_2O. (c) Hydrodynamic diameters of the siRNA−PEI polyplexes (PEI:siRNA weight ratio = 0.3 and 1) with the gradual addition of miRNA, as measured in 150 mM KCl. (d) The ζ-potential of the siRNA−PEI polyplexes with the gradual addition of miRNA. For PEI:RNA weight ratios of 0.3 and 1, the corresponding N:P ratios are 2.37 and 7.90, respectively.

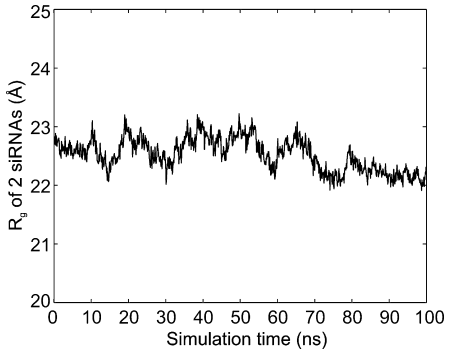

Figure 10. R_g of the two siRNAs in the 2s-4P-4m system as a function of simulation time.

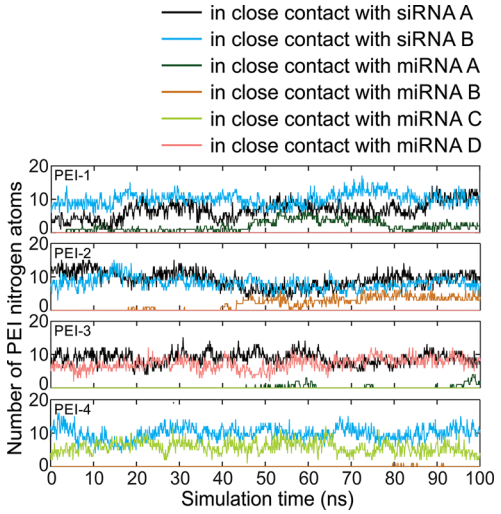

Figure 11. Number of Ns for each PEI within 4 Å of each siRNA and miRNA N/O atom as a function of simulation time. The four plots in each subfigure correspond to four PEIs, and the six curves in each plot correspond to two siRNAs and four miRNAs in the 2s-4P-4m system.

section 3.1. The four plots in each subfigure again correspond to the four PEIs in the system, while six curves are present in each plot, representing the six RNA molecules, two siRNA and four miRNA. Previously, in system 2s-4P, PEI-1 and PEI-2 were found to bridge siRNA A and B (Figure 6a). In Figure 11, it is clear that these two PEIs continue to bridge the two siRNAs, and the numbers of PEI N's in close contact with the siRNAs have not decreased after miRNA contact. In fact, for PEI-1, the numbers of N's in close contact with the siRNAs, averaged over the last 20 ns, are, respectively, 9 and 10 for siRNA A and B. These numbers are even slightly larger than the average numbers (over the last 10 ns) found for system 2s-4P before the introduction of miRNAs, which are 4 and 7. As in system 2s-4P, PEI-3 and PEI-4 do not participate in polyion bridging and are only bound to one siRNA. In addition to maintaining the same binding pattern with siRNA, new contacts are established between PEIs and miRNAs. In particular, PEI-1 is

DOI: 10.1021/acs.jpcb.5b00415
J. Phys. Chem. B 2015, 119, 5475−5486

bound to miRNA A, thereby simultaneously bridging three RNAs, two siRNA and one miRNA. PEI-2 bridges the two siRNA as well as miRNA B. PEI-3 started to bridge siRNA A and miRNA D; additionally, short-term transient bridges with miRNA A are observed (between 50 and 60 ns, between 70 and 80 ns, and after 90 ns). Similarly, PEI-4 bridges siRNA B and miRNA C, and forms short-term transient bridges with miRNA B (between 80 and 90 ns). These results show that introduction of miRNA not only conserved the overall binding pattern of PEI to siRNA but also allowed the formation of new polyion bridges between siRNA and miRNA molecules, which clearly demonstrate the ability of PEI to accommodate additional RNAs.

To examine the change in the screening of siRNA charges upon miRNA introduction, cumulative distributions of PEI N^+, K^+, and Cl^- and miRNA P^- atoms as well as their total net charge are plotted as a function of the distance from any siRNA C1′ atom, averaged over the last 20 ns of the simulation (Figure 12). The black solid line indicates the cumulative number of

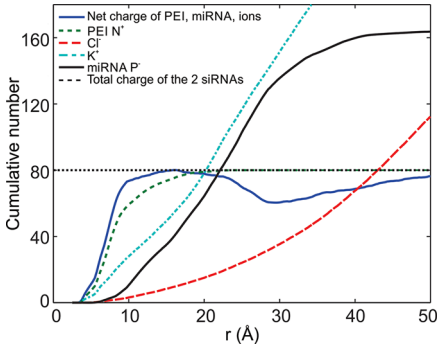

Figure 12. Cumulative numbers of PEI N^+, K^+, and Cl^- and miRNA P^- atoms and the total net charge of PEI, miRNA, and ions as a function of the distance from any siRNA C1′ atoms, averaged over the last 20 ns of the 2s-4P-4m simulation. A total charge of −80 of the two siRNAs is plotted by a black dashed line as a reference.

miRNA P^-'s as a function of distance from siRNA C1′'s, while the rest of the curves are represented in the same way as in Figure 7a. miRNA charges follow an increasing trend, and at large distances, 49−50 Å, they reach up to their total charge of −164. No considerable change is observed in the number of PEI N^+'s upon miRNA introduction, while the K^+ charges increase more rapidly to accommodate the excessive negative charge coming from miRNA P^-'s. 100% neutralization of siRNA charges occurs at 15.98 Å, which is almost identical to that reported in the 2s-4P system (15.99 Å). On the other hand, the overneutralization seen in the 2s-4P system is no longer observed. Excessive negative charge of miRNA led to the formation of an overall negatively charged complex structure, indicated by the fact that the solid blue curve decreases beyond the neutralization distance and is never above the black dashed line.

To summarize, for the simulated system where the miRNA:siRNA mole ratio is set to 2 and within the simulation time of 100 ns, the miRNAs were not observed to affect the integrity of the siRNA−PEI polyplex. This is in agreement with the experimental data presented earlier. In contrast to our initial speculation that the stronger binding between miRNA and PEI might lead to dissociation of siRNA polyplexes in the presence of miRNAs, our experimental and computational results showed that PEIs are capable of bridging the miRNAs to the siRNA−PEI polyplex and forming an additional miRNA layer.

3.3. Limitations. PEI simulated in this study has a protonation state of 47%, corresponding to the experimentally determined value at pH 6.[27] Most computational studies involving protonable carriers adopted this approach, where the carrier's protonation ratio is specified at a certain value in the beginning and remains the same throughout the simulation.[42−44] A more realistic way is to perform constant pH simulations in which the carrier's protonation state is allowed to vary while the pH is kept constant. Although this approach is closer to realistic conditions, due to the current computational limitations, most reported constant pH simulations treated the solvent implicitly.[45−47] Since water dynamics, i.e., water release upon complexation and H-bonding, constitutes an important part of the polynucleotide−carrier binding dynamics,[28] implicit solvent methods cannot provide accurate descriptions on the complexation mechanism.[48] This barrier is being removed with emerging methodologies to treat solvent explicitly[49−51] in constant pH simulations.

In this study, we simulated a low molecular weight (LMW) PEI molecule (2 kDa), since current computational limitations do not allow us to simulate high molecular weight (HMW) PEI structures such as 25 kDa PEI widely used in experiments. On the other hand, we believe that the complexation dynamics should also be applicable to HMW PEIs.[29] It also has to be noted that, studies have reported LMW PEIs as effective as HMW PEIs and yet less toxic, with the substitution of hydrophobic moieties into PEI's structure.[52]

Another limitation is the size and time scale of the simulation system. Although we reported nanoparticles in experiments having hydrodynamic diameters of 517 ± 32 nm for siRNA−PEI and 635 ± 48 nm for miRNA−PEI systems at a PEI:RNA weight ratio of 0.3 (Figure 9a), the corresponding particle sizes are 5−6 nm in the simulations. With the current computational capabilities, it is not practical to simulate a system which is hundreds of nanometers in size. Despite the smaller size of our systems, we believe that our simulations should capture the fundamental complexation mechanism at the atomistic level. In terms of time, in reality, formation and dissociation of siRNA polyplexes occur on the scale of minutes (<1 h), while current computational capabilities allow simulations up to μs in the atomistic scale. Although length and time constraints can be overcome with other approaches such as coarse grain (CG) simulations, lack of atomistic information may lead to inaccurate results in this case. Our binding simulations in this study were performed for 50 ns, which are longer than most of the all-atom simulations reported on the binding of biomolecules, e.g., typically 4−26 ns for polycation binding to siRNA[42,44,53−58] and 12−20 ns to DNA.[59,60] To our knowledge, there have not been any all-atom MD simulations probing the dissociation of siRNA polyplexes and/or the effect of anionic endogenous molecules on the integrity of siRNA polyplexes. Unlike binding, our simulations inspecting the effect of miRNA on the integrity of the siRNA−PEI polyplex are longer (100 ns), but it is possible that they might still be too short to capture the most probable configuration of the siRNA polyplex upon the addition of miRNA, if the simulated system is trapped in a potential energy well. However, it should be emphasized that the conclusion made on the effect of miRNA (i.e., absence of dissociation and formation of a siRNA−PEI−miRNA ternary complex) is not solely based on the simulations. Our EMSA and ζ-potential analysis provided

DOI: 10.1021/acs.jpcb.5b00415
J. Phys. Chem. B 2015, 119, 5475−5486

direct evidence for such phenomena, while MD simulation validated the experimental observations giving atomistic details on the interaction of miRNA with the siRNA−PEI polyplex. Given the current computational limitations, it is encouraging to see that our simulations provided a good agreement with the experimental observations. Restrained MD simulations, e.g., steered molecular dynamics (SMD) (see, for example, refs 61 and 62), coupled with potential of mean force measurements may be used to better quantify the dissociation capability of other anionic molecules, but this is out of the scope of the present work.

Finally, in our simulations, we only adopted two initial configurations of the siRNA−PEI polyplex (one presented in Figure 3a (left and middle panels) and the other in Figure S2 of the Supporting Information), for the simulations on polyplex formation as well as for probing the effect of miRNA on the polyplex integrity. Although these initial configurations led to quantitatively different results, e.g., 0.87 Å difference in radius of gyration of siRNA−PEI polyplex, the qualitative outcomes are similar. Practically, it is not possible to examine all initial configurations with MD simulations; therefore, the structures observed at the end of our simulations are only some of the possible configurations that can be formed by these molecules. However, the good agreement found between simulations and experimental ζ-potential measurements, i.e., positively charged particles formed by siRNA and/or miRNA with PEI and negatively charged particles formed upon gradual miRNA addition onto siRNA−PEI polyplexes, indicates these final structures are highly probable configurations.

3.4. Implications and Future Studies. Through endocytosis and endosomal escape, the strength of interaction between the siRNA and carriers is likely to be weakened, causing the polyplexes to be more prone to dissociation. Electrostatic attraction between anionic endogenous molecules such as oligonucleotides and cationic carriers in polyplexes might play a role in affecting polyplex integrity in cytosol. The effect of miRNA on siRNA−PEI polyplexes derived from our MD simulations revealed the formation of a layered structure on siRNA−PEI polyplexes. Whether varying size, charge, or structure of miRNA makes any further impact on the stability of siRNA polyplexes should be assessed with future MD simulations and experiments, given the diversity on miRNA structures. While further research to probe the effect of other endogenous molecules on siRNA polyplexes is warranted, our results can give some insights on how stable the polyplexes are against anionic molecules in cytosol, as well as how polyplex charge and size are affected by these substances.

The ability of PEI to accommodate excessive anionic charge coming from another RNA and to form a layer surrounding the existing polyplex makes it possible to gain insight into "layer-by-layer (LbL) assembled polyplexes". LbL is a recent technique used in the design of delivery systems. LbL coated gold nanoparticles for the delivery of siRNA[63−65] and poly(lactide-*co*-glycolide) (PLGA) microparticles for the delivery of DNA[66] have been reported. LbL assembled polyplexes may facilitate more controlled loading of siRNA into complexes. Thus, MD simulations could be employed to assess the material properties of such structures as well as the siRNA loading efficiency of the reported structures.

The effect of some polyanionic molecules on the integrity of polynucleotide complexes has been reported in the literature. Albumin was shown not to release DNA from its complex with polycations, and instead, it was bound to preformed DNA−polycation complexes and induced formation of a ternary structure.[67] Similarly, introduction of anionic polymer, poly(γ-glutamic acid) (γ-PGA), into DNA−chitosan complexes resulted in a ternary complex structure, with a DNA−chitosan core and a surrounding γ-PGA layer.[68] In the same work, MD simulations on DNA−chitosan−γ-PGA showed the binding of anionic γ-PGA to the DNA−chitosan complex, through the interactions with available cationic chitosan molecules. Similar to our observations made when introducing excess miRNA to FAM−siRNA−PEI polyplexes, introduction of excess amounts of γ-PGA into the DNA−chitosan complex resulted in excess γ-PGA suspending freely in solution. In addition, an increase in the transfection efficiency with γ-PGA coating was also reported, although it was attributed to a specific protein mediated endocytosis. As an anionic molecule to coat the polynucleotide complexes, hyaluronic acid (HA) has attracted more attention due to its biocompatible and biodegradable nature. HA coating was reported to reduce cytotoxicity of polyplexes, and increase transfection efficiency, possibly due to HA receptor mediated endocytosis.[69,70] Future *in vitro* experimental studies might be beneficial to determine if the addition of miRNA might alter cytotoxicity and transfection of polyplexes.

4. CONCLUSIONS

We performed experimental binding studies and a series of all-atom MD simulations to study PEI binding to siRNA and miRNA, and the effect of miRNA addition on the integrity of siRNA−PEI polyplexes. EMSA and SYBR Green II dye exclusion assays along with individual complexation simulations with miRNA and siRNA revealed PEI's slightly better binding to miRNA. Despite the observed better binding, from EMSA and SYBR Green II dye exclusion assays, we found that miRNA introduction into a preformed siRNA−PEI polyplex failed to break the preformed interactions between the siRNA and PEI. This is confirmed by MD simulations where additional miRNA was observed to bind to the preformed siRNA polyplex through the electrostatic interactions with the accessible PEI, and formed an additional surrounding layer without weakening the interactions already formed between siRNA and PEI. The resulting structure observed from MD simulation, an overall negatively charged ternary complex comprising a core of siRNA−PEI polyplex and an outer layer of miRNA, is consistent with the experimental finding that the ζ-potential of the particle decreases upon gradual addition of miRNA.

■ ASSOCIATED CONTENT

Ⓢ Supporting Information

miRNA was pre-equilibrated, and the simulation trajectory was analyzed for structural changes. Different initial configurations were tested to probe the effect of initial structures on the simulation systems. The ζ-potentials of the siRNA−PEI and miRNA−PEI polyplexes were measured at different PEI:RNA weight ratios. This material is available free of charge via the Internet at http://pubs.acs.org.

■ AUTHOR INFORMATION

Corresponding Authors

*E-mail: tian.tang@ualberta.ca.
*E-mail: hasan.uludag@ualberta.ca.

Notes

The authors declare no competing financial interest.

DOI: 10.1021/acs.jpcb.5b00415
J. Phys. Chem. B 2015, 119, 5475−5486

■ ACKNOWLEDGMENTS

Computing resources and technical support from Compute Canada and the high performance computing facility at National Institute for Nanotechnology, Edmonton, Canada, were gratefully acknowledged. This work is funded by Natural Sciences and Engineering Research Council of Canada (T.T. and H.U.), Canadian Institutes of Health Research (H.U.), Alberta Innovates Health Solutions (H.U.), Alberta Innovates-Technology Futures (T.T.), and Canada Foundation for Innovation (T.T.). We thank Dr. Afsaneh Lavasanifar (Faculty of Pharmacy & Pharmaceutical Sciences) for access to the Zetasizer.

■ REFERENCES

(1) Fire, A.; Xu, S.; Montgomery, M. K.; Kostas, S. A.; Driver, S. E.; Mello, C. C. Potent and Specific Genetic Interference by Double-stranded RNA in Caenorhabditis Elegans. *Nature* **1998**, *391*, 806−811.
(2) Davidson, B. L.; McCray, P. B., Jr. Current Prospects for RNA Interference-based Therapies. *Nat. Rev. Genet.* **2011**, *12*, 329−340.
(3) Zhang, S.; Zhao, B.; Jiang, H.; Wang, B.; Ma, B. Cationic Lipids and Polymers Mediated Vectors for Delivery of siRNA. *J. Controlled Release* **2007**, *123*, 1−10.
(4) Boussif, O.; Lezoualc'h, F.; Zanta, M. A.; Mergny, M. D.; Scherman, D.; Demeneix, B.; Behr, J. P. A Versatile Vector for Gene and Oligonucleotide Transfer into Cells in Culture and In vivo: Polyethylenimine. *Proc. Natl. Acad. Sci. U.S.A.* **1995**, *92*, 7297−7301.
(5) Dominska, M.; Dykxhoorn, D. M. Breaking Down the Barriers: siRNA Delivery and Endosome Escape. *J. Cell Sci.* **2010**, *123*, 1183−1189.
(6) Czech, B.; Hannon, G. J. Small RNA Sorting: Matchmaking for Argonautes. *Nat. Rev. Genet.* **2011**, *12*, 19−31.
(7) Ding, H. M.; Ma, Y. Q. Role of Physicochemical Properties of Coating Ligands in Receptor-mediated Endocytosis of Nanoparticles. *Biomaterials* **2012**, *33*, 5798−5802.
(8) Ding, H. M.; Ma, Y. Q. Design Maps for Cellular Uptake of Gene Nanovectors by Computer Simulation. *Biomaterials* **2013**, *34*, 8401−8407.
(9) Ding, H. M.; Ma, Y. Q. Controlling Cellular Uptake of Nanoparticles with pH-sensitive Polymers. *Sci. Rep.* **2013**, *3*, 2804.
(10) Dinh, A. T.; Pangarkar, C.; Theofanous, T.; Mitragotri, S. Understanding Intracellular Transport Processes Pertinent to Synthetic Gene Delivery via Stochastic Simulations and Sensitivity Analyses. *Biophys. J.* **2007**, *92*, 831−846.
(11) Gilleron, J.; Querbes, W.; Zeigerer, A.; Borodovsky, A.; Marsico, G.; Schubert, U.; Manygoats, K.; Seifert, S.; Andree, C.; Stoter, M.; et al. Image-based Analysis of Lipid Nanoparticle-mediated siRNA Delivery, Intracellular Trafficking and Endosomal Escape. *Nat. Biotechnol.* **2013**, *31*, 638−646.
(12) Sahay, G.; Querbes, W.; Alabi, C.; Eltoukhy, A.; Sarkar, S.; Zurenko, C.; Karagiannis, E.; Love, K.; Chen, D. L.; Zoncu, R.; et al. Efficiency of siRNA Delivery by Lipid Nanoparticles is Limited by Endocytic Recycling. *Nat. Biotechnol.* **2013**, *31*, 653−658.
(13) Behr, J. P. The Proton Sponge: A Trick to Enter Cells the Viruses Did Not Exploit. *Chimia* **1997**, *51*, 34−36.
(14) Benjaminsen, R. V.; Mattebjerg, M. A.; Henriksen, J. R.; Moghimi, S. M.; Andresen, T. L. The Possible "Proton Sponge" Effect of Polyethylenimine (PEI) Does Not Include Change in Lysosomal pH. *Mol. Ther.* **2013**, *21*, 149−157.
(15) Won, Y. Y.; Sharma, R.; Konieczny, S. F. Missing Pieces in Understanding the Intracellular Trafficking of Polycation/DNA Complexes. *J. Controlled Release* **2009**, *139*, 88−93.
(16) Sasisekharan, R.; Shriver, Z.; Venkataraman, G.; Narayanasami, U. Roles of Heparan-Sulphate Glycosaminoglycans in Cancer. *Nat. Rev. Cancer* **2002**, *2*, 521−528.
(17) Xu, Y. H.; Szoka, F. C. Mechanism of DNA Release from Cationic Liposome/DNA Complexes Used in Cell Transfection. *Biochemistry* **1996**, *35*, 5616−5623.
(18) Ruponen, M.; Yla-Herttuala, S.; Urtti, A. Interactions of Polymeric and Liposomal Gene Delivery Systems with Extracellular Glycosaminoglycans: Physicochemical and Transfection Studies. *Biochim. Biophys. Acta* **1999**, *1415*, 331−341.
(19) Moret, I.; Esteban Peris, J.; Guillem, V. M.; Benet, M.; Revert, F.; Dasi, F.; Crespo, A.; Alino, S. F. Stability of PEI-DNA and DOTAP-DNA Complexes: Effect of Alkaline pH, Heparin and Serum. *J. Controlled Release* **2001**, *76*, 169−181.
(20) Ruponen, M.; Honkakoski, P.; Ronkko, S.; Pelkonen, J.; Tammi, M.; Urtti, A. Extracellular and Intracellular Barriers in Non-viral Gene Delivery. *J. Controlled Release* **2003**, *93*, 213−217.
(21) Aliabadi, H. M.; Landry, B.; Sun, C.; Tang, T.; Uludag, H. Supramolecular Assemblies in Functional siRNA Delivery: Where Do We Stand? *Biomaterials* **2012**, *33*, 2546−2569.
(22) Calin, G. A.; Croce, C. M. MicroRNA Signatures in Human Cancers. *Nat. Rev. Cancer* **2006**, *6*, 857−866.
(23) Esquela-Kerscher, A.; Slack, F. J. Oncomirs - MicroRNAs with a Role in Cancer. *Nat. Rev. Cancer* **2006**, *6*, 259−269.
(24) Lagos-Quintana, M.; Rauhut, R.; Lendeckel, W.; Tuschl, T. Identification of Novel Genes Coding for Small Expressed RNAs. *Science* **2001**, *294*, 853−858.
(25) Krichevsky, A. M.; Gabriely, G. miR-21: A Small Multi-faceted RNA. *J. Cell. Mol. Med.* **2009**, *13*, 39−53.
(26) Abbasi, M.; Lavasanifar, A.; Berthiaume, L. G.; Weinfeld, M.; Uludag, H. Cationic Polymer-mediated Small Interfering RNA Delivery for P-glycoprotein Down-regulation in Tumor Cells. *Cancer* **2010**, *116*, 5544−5554.
(27) Utsuno, K.; Uludag, H. Thermodynamics of Polyethlyenimine-DNA Binding and DNA Condensation. *Biophys. J.* **2010**, *99*, 201−207.
(28) Sun, C.; Tang, T.; Uludag, H. A Molecular Dynamics Simulation Study on the Effect of Lipid Substitution on Polyethylenimine Mediated siRNA Complexation. *Biomaterials* **2013**, *34*, 2822−2833.
(29) Sun, C.; Tang, T.; Uludag, H.; Cuervo, J. E. Molecular Dynamics Simulations of DNA/PEI Complexes: Effect of PEI Branching and Protonation State. *Biophys. J.* **2011**, *100*, 2754−2763.
(30) Vanommeslaeghe, K.; Hatcher, E.; Acharya, C.; Kundu, S.; Zhong, S.; Shim, J.; Darian, E.; Guvench, O.; Lopes, P.; Vorobyov, I.; et al. CHARMM General Force Field: A Force Field for Drug-like Molecules Compatible with the CHARMM All-atom Additive Biological Force Fields. *J. Comput. Chem.* **2010**, *31*, 671−690.
(31) Brooks, B. R.; Bruccoleri, R. E.; Olafson, B. D.; States, D. J.; Swaminathan, S.; Karplus, M. Charmm − A Program for Macromolecular Energy, Minimization, and Dynamics Calculations. *J. Comput. Chem.* **1983**, *4*, 187−217.
(32) MacKerell, A. D.; Brooks, B.; Brooks, C. L.; Nilsson, L.; Roux, B.; Won, Y.; Karplus, M., CHARMM: The Energy Function and Its Parameterization with an Overview of the Program. In *The Encyclopedia of Computational Chemistry*; John Wiley & Sons: Chichester, U.K., 1998; pp 271−277.
(33) Foloppe, N.; MacKerell, A. D., Jr. All-Atom Empirical Force Field for Nucleic Acids: I. Parameter Optimization Based on Small Molecule and Condensed Phase Macromolecular Target Data. *J. Comput. Chem.* **2000**, *21*, 86−104.
(34) MacKerell, A. D.; Banavali, N. K. All-atom Empirical Force Field for Nucleic Acids: II. Application to Molecular Dynamics Simulations of DNA and RNA in Solution. *J. Comput. Chem.* **2000**, *21*, 105−120.
(35) Phillips, J. C.; Braun, R.; Wang, W.; Gumbart, J.; Tajkhorshid, E.; Villa, E.; Chipot, C.; Skeel, R. D.; Kale, L.; Schulten, K. Scalable Molecular Dynamics with NAMD. *J. Comput. Chem.* **2005**, *26*, 1781−1802.
(36) Jorgensen, W. L. Quantum and Statistical Mechanical Studies of Liquids. 10. Transferable Intermolecular Potential Functions for Water, Alcohols, and Ethers - Application to Liquid Water. *J. Am. Chem. Soc.* **1981**, *103*, 335−340.
(37) Balasubramanian, C.; Ojha, R. P.; Maiti, S.; Desideri, A. Sampling the Structure of the Noncanonical lin-4:lin-14 microRNA:mRNA Complex by Molecular Dynamics Simulations. *J. Phys. Chem. B* **2010**, *114*, 16443−16449.

DOI: 10.1021/acs.jpcb.5b00415
J. Phys. Chem. B 2015, 119, 5475−5486

(38) Darden, T.; York, D.; Pedersen, L. Particle Mesh Ewald: An N·log(N) Method for Ewald Sums in Large Systems. *J. Chem. Phys.* **1993**, *98*, 10089−10092.
(39) Ryckaert, J. P.; Ciccotti, G.; Berendsen, H. J. C. Numerical Integration of the Cartesian Equations of Motion of a System with Constraints: Molecular Dynamics of N-alkanes. *J. Comput. Phys.* **1977**, *23*, 327−341.
(40) Humphrey, W.; Dalke, A.; Schulten, K. VMD: Visual Molecular Dynamics. *J. Mol. Graphics* **1996**, *14*, 33−38.
(41) Sun, C.; Tang, T.; Uludag, H. Molecular Dynamics Simulations of PEI Mediated DNA Aggregation. *Biomacromolecules* **2011**, *12*, 3698−3707.
(42) Ouyang, D.; Zhang, H.; Parekh, H. S.; Smith, S. C. The Effect of pH on PAMAM Dendrimer-siRNA Complexation: Endosomal Considerations as Determined by Molecular Dynamics Simulation. *Biophys. Chem.* **2011**, *158*, 126−133.
(43) Pavan, G. M.; Posocco, P.; Tagliabue, A.; Maly, M.; Malek, A.; Danani, A.; Ragg, E.; Catapano, C. V.; Pricl, S. PAMAM Dendrimers for siRNA Delivery: Computational and Experimental Insights. *Chemistry* **2010**, *16*, 7781−7795.
(44) Karatasos, K.; Posocco, P.; Laurini, E.; Pricl, S. Poly-(amidoamine)-based Dendrimer/siRNA Complexation Studied by Computer Simulations: Effects of pH and Generation on Dendrimer Structure and siRNA Binding. *Macromol. Biosci.* **2012**, *12*, 225−240.
(45) Khandogin, J.; Brooks, C. L. Constant pH Molecular Dynamics with Proton Tautomerism. *Biophys. J.* **2005**, *89*, 141−157.
(46) Baptista, A. M.; Teixeira, V. H.; Soares, C. M. Constant-pH Molecular Dynamics Using Stochastic Titration. *J. Chem. Phys.* **2002**, *117*, 4184−4200.
(47) Mongan, J.; Case, D. A.; McCammon, J. A. Constant pH Molecular Dynamics in Generalized Born Implicit Solvent. *J. Comput. Chem.* **2004**, *25*, 2038−2048.
(48) Meneksedag-Erol, D.; Tang, T.; Uludag, H. Molecular Modeling of Polynucleotide Complexes. *Biomaterials* **2014**, *35*, 7068−7076.
(49) Wallace, J. A.; Shen, J. K. Continuous Constant pH Molecular Dynamics in Explicit Solvent with pH-Based Replica Exchange. *J. Chem. Theory Comput.* **2011**, *7*, 2617−2629.
(50) Goh, G. B.; Knight, J. L.; Brooks, C. L. Constant pH Molecular Dynamics Simulations of Nucleic Acids in Explicit Solvent. *J. Chem. Theory Comput.* **2012**, *8*, 36−46.
(51) Donnini, S.; Tegeler, F.; Groenhof, G.; Grubmuller, H. Constant pH Molecular Dynamics in Explicit Solvent with Lambda-Dynamics. *J. Chem. Theory Comput.* **2011**, *7*, 1962−1978.
(52) Aliabadi, H. M.; Landry, B.; Bahadur, R. K.; Neamnark, A.; Suwantong, O.; Uludag, H. Impact of Lipid Substitution on Sssembly and Delivery of siRNA by Cationic Polymers. *Macromol. Biosci.* **2011**, *11*, 662−672.
(53) Pavan, G. M.; Albertazzi, L.; Danani, A. Ability to Adapt: Different Generations of PAMAM Dendrimers Show Different Behaviors in Binding siRNA. *J. Phys. Chem. B* **2010**, *114*, 2667−2675.
(54) Pavan, G. M.; Kostiainen, M. A.; Danani, A. Computational Approach for Understanding the Interactions of UV-degradable Dendrons with DNA and siRNA. *J. Phys. Chem. B* **2010**, *114*, 5686−5693.
(55) Jensen, L. B.; Mortensen, K.; Pavan, G. M.; Kasimova, M. R.; Jensen, D. K.; Gadzhyeva, V.; Nielsen, H. M.; Foged, C. Molecular Characterization of the Interaction between siRNA and PAMAM G7 Dendrimers by SAXS, ITC, and Molecular Dynamics Simulations. *Biomacromolecules* **2010**, *11*, 3571−3577.
(56) Ouyang, D.; Zhang, H.; Parekh, H. S.; Smith, S. C. Structure and Dynamics of Multiple Cationic Vectors-siRNA Complexation by All-atomic Molecular Dynamics Simulations. *J. Phys. Chem. B* **2010**, *114*, 9231−9237.
(57) Ouyang, D.; Zhang, H.; Herten, D. P.; Parekh, H. S.; Smith, S. C. Structure, Dynamics, and Energetics of siRNA-Cationic Vector Complexation: A Molecular Dynamics Study. *J. Phys. Chem. B* **2010**, *114*, 9220−9230.
(58) Vasumathi, V.; Maiti, P. K. Complexation of siRNA with Dendrimer: A Molecular Modeling Approach. *Macromolecules* **2010**, *43*, 8264−8274.
(59) Ziebarth, J.; Wang, Y. Molecular Dynamics Simulations of DNA-Polycation Complex Formation. *Biophys. J.* **2009**, *97*, 1971−1983.
(60) Elder, R. M.; Emrick, T.; Jayaraman, A. Understanding the Effect of Polylysine Architecture on DNA Binding Using Molecular Dynamics Simulations. *Biomacromolecules* **2011**, *12*, 3870−3879.
(61) Kosztin, D.; Izrailev, S.; Schulten, K. Unbinding of Retinoic Acid from Its Receptor Studied by Steered Molecular Dynamics. *Biophys. J.* **1999**, *76*, 188−197.
(62) Martinez, L.; Sonoda, M. T.; Webb, P.; Baxter, J. D.; Skaf, M. S.; Polikarpov, I. Molecular Dynamics Simulations Reveal Multiple Pathways of Ligand Dissociation from Thyroid Hormone Receptors. *Biophys. J.* **2005**, *89*, 2011−2023.
(63) Elbakry, A.; Zaky, A.; Liebl, R.; Rachel, R.; Goepferich, A.; Breunig, M. Layer-by-layer Assembled Gold Nanoparticles for siRNA Delivery. *Nano Lett.* **2009**, *9*, 2059−2064.
(64) Guo, S.; Huang, Y.; Jiang, Q.; Sun, Y.; Deng, L.; Liang, Z.; Du, Q.; Xing, J.; Zhao, Y.; Wang, P. C.; et al. Enhanced Gene Delivery and siRNA Silencing by Gold Nanoparticles Coated with Charge-reversal Polyelectrolyte. *ACS Nano* **2010**, *4*, 5505−5511.
(65) Song, W. J.; Du, J. Z.; Sun, T. M.; Zhang, P. Z.; Wang, J. Gold Nanoparticles Capped with Polyethyleneimine for Enhanced siRNA Delivery. *Small* **2010**, *6*, 239−246.
(66) Kakade, S.; Manickam, D. S.; Handa, H.; Mao, G.; Oupicky, D. Transfection Activity of Layer-by-Layer Plasmid DNA/poly-(ethylenimine) Films Deposited on PLGA Microparticles. *Int. J. Pharm.* **2009**, *365*, 44−52.
(67) Oupicky, D.; Konak, C.; Dash, P. R.; Seymour, L. W.; Ulbrich, K. Effect of Albumin and Polyanion on the Structure of DNA Complexes with Polycation Containing Hydrophilic Nonionic Block. *Bioconjugate Chem.* **1999**, *10*, 764−772.
(68) Liao, Z. X.; Peng, S. F.; Ho, Y. C.; Mi, F. L.; Maiti, B.; Sung, H. W. Mechanistic Study of Transfection of Chitosan/DNA Complexes Coated by Anionic Poly(gamma-glutamic acid). *Biomaterials* **2012**, *33*, 3306−3315.
(69) Ito, T.; Iida-Tanaka, N.; Koyama, Y. Efficient In Vivo Gene Transfection by Stable DNA/PEI Complexes Coated by Hyaluronic Acid. *J. Drug Targeting* **2008**, *16*, 276−281.
(70) He, Y.; Cheng, G.; Xie, L.; Nie, Y.; He, B.; Gu, Z. Polyethyleneimine/DNA Polyplexes with Reduction-sensitive Hyaluronic Acid Derivatives Shielding for Targeted Gene Delivery. *Biomaterials* **2013**, *34*, 1235−1245.

DOI: 10.1021/acs.jpcb.5b00415
J. Phys. Chem. B 2015, 119, 5475−5486